Reflectance Spectra of Munsell Standard Chips and Their Appearance

Tarow Indow, A. Kimball Romney*

School of Social Sciences, University of California Irvine, Irvine, CA 92697

Received 29 January 2006; revised 17 July 2007; accepted 7 September 2007

Abstract: In this article, we present the results of analysis by two different methods for representing information in reflectance spectra of Munsell standard chips that relates to their appearance. The spectrum of a chip j is denoted as $r_{j\mu}$ where μ represents wavelength λ from 430 to 660 nm with 1 nm intervals. The spectrum of light reflected from a chip j under D65 is $r_{j\mu} \times e_\mu$ where e_μ represents the spectral power distribution of D65 illumination. In one method, singular value decomposition is applied to a matrix of $(r_{j\mu} \times e_\mu)$. Combining results of this analysis with results of human assessment experiments, we obtain four curves $\xi_{0\alpha}(H)$ that represent principal hue components α in Munsell Hue, α = redness, yellowness, greenness, and blueness (Fig. 6). The other method is multiple regression of each $(r_{j\mu} \times e_\mu)$ to activities of three kinds of cones in the retina. From this analysis, we obtain three curves $B_q(H)$ that represent relative involvements of q = L, M, S cone activities in determining the appearance of Munsell Hue (Fig. 10). Two sets of curves, $\xi_{0\alpha}(H)$, and $B_q(H)$, are compared with predictions from a model of higher order color mechanism (Fig. 12) that has been proposed on the basis of experiments with light stimuli of wavelength λ. It is found that $\xi_{0\alpha}(H)$, and $B_q(H)$ constructed from broadband spectra of Munsell chips are interpretable in terms of this model. © 2008 Wiley Periodicals, Inc. Col Res Appl, 33, 229–237, 2008; Published online in Wiley InterScience (www.interscience.wiley.com). DOI 10.1002/col.20406

Key words: color appearance model; color scaling; cone activities; Munsell system; singular value decomposition

INTRODUCTION

The Munsell color system is a framework for specifying the appearance of a surface color in terms of three coordinates: Hue (H), Chroma (C), and Value (V). Munsell standard color chips are represented in a cylindrical coordinate system. The vertical axis represents V changing from black to white through gray. The polar coordinates represent H (polar angle) and C (polar distance). In each coordinate, standard color chips are defined to form a series of equal-appearing-intervals with its own unit: V varies from 0 (the ideal black) to 10 (the ideal white), whereas C varies from 0 (achromatic color) to an integer, for example, 12, representing the most saturated color of given H and V. The hue circle—from red through yellow, green, blue, purple to red—is divided into 10 regions. The 10 regions represent the five primary Munsell hues, R, Y, G, B, and P, plus five intermediate hues, YR, GY, BG, PB, and RP. In each hue region, H is normally denoted by four areas: 2.5, 5, 7.5, and 10, for example, 2.5R, 5R, 7.5R, 10R. Area five usually represents the most representative hue. It is not guaranteed that one step in V, one step in C, and one step in H represent the same size of perceptual difference. Arranging standard color chips in each coordinate as a series of equal-appearing-intervals with its own unit is sufficient to uniquely specify a surface color as (H V/C) by visually comparing it with this framework. Perceptual interpolation will be easy with a series of equal-appearing-intervals and, for instance, V can be denoted by any value between 0 and 10. However, we need a special consideration to relate the size of difference δ_{jk} that we perceive between two colors j and k differing in more than one attribute to the distance between two points (H_j V_j/C_j) and (H_k V_k/C_k) in the Munsell color solid.

Perceptual Color Difference δ

As to Munsell color solid, Indow[1,2] obtained the following results with regard to δ_{jk}.

*Correspondence to: A. Kimball Romney (e-mail: akromney@hermes.ss.uci.edu).

(D1): Perceived color difference δ_{jk} is a latent variable. However, observers can match its size with a perceived achromatic difference between two gray chips, A and B, in the V scale, provided that δ_{jk} is limited within a certain range. Hence δ_{jk} can be converted to an observable variable $d_{jk} = |V_A - V_B|$. This scale d of δ has the Munsell V unit. The range in which this matching is made with confidence is such a size of δ that is scaled as d between 0 and $3.5V$. For this reason, a data matrix $\mathbf{D} = (d_{jk})$ has a number of vacant cells.

(D2): By series of application of multidimensional scaling to matrix $\mathbf{D} = (d_{jk})$ of an appropriate number of chips sampled from the main part of Munsell color solid, it was shown that standard chips can be represented as a 3D configuration of points $\{P_j\}$ in which local Euclidean distance $\hat{d}_{jk}$ between P_j and P_k in this configuration is proportional to data d_{jk}. When d_{jk} are plotted against $\hat{d}_{jk}$, points are along a straight line passing through the origin with the scatter in the order of $0.23V$. This is only about three times of just-noticeable difference of lightness on the scale V.

(D3): The configuration $\{P_j\}$ obtained from a $\mathbf{D}$ reproduces the global structure of Munsell color solid $\{P_j\}_M$. We can identify such an axis that corresponds to V and such a plane perpendicular to V that corresponds to (H, C). Throughout $\{P_j\}$'s from $\mathbf{D}$'s of various multidimensional scaling experiments, one step in this V axis is equivalent to 2.3 step in this C coordinate.

(D4): If data d_{jk} are plotted against Euclidean distance between $P_j(H_j\ V_j/C_j)$ and $P_k(H_k\ V_k/C_k)$ in the Munsell color solid $\{P_j\}_M$ under the condition that $1V = 2.3C$, points are along a straight line passing through the origin with the scatter in the order of $0.6V$.

Thus, it was shown that Munsell color chips are embeddable in a 3D space as a configuration of points $\{P_j\}$ with a unified unit. Because of (D1), the space is locally Euclidean at least. However, the structure of $\{P_j\}$ constructed by multidimensional scaling does not exactly coincide with that of Munsell color solid $\{P_j\}_M$, and we cannot tell to what extent the discrepancies are ascribed to inadequacy of $\{P_j\}_M$ as a configuration representing δ_{jk} and to what extent these are due to distortion of a constructed configuration $\{P_j\}$ that is caused by bias in sampling j, k to have a $\mathbf{D} = (d_{jk})$ that inevitably has many vacant cells. It is difficult to obtain such a $\{P_j\}$ that is completely free from possible distortion. Hence, Indow shifted the direction of research from modifying $\{P_j\}_M$ so as to have a unified color difference metric to examination of the status quo of Munsell standard chips. First, the appearance of each chip j was examined.

Perceptual Color Appearance $\mathcal{H}$

Let us denote by $\mathcal{H}_\alpha(j)$ the degree of principal hue α we see in each standard color chip j. For example, we see redness and yellowness in an orange color chip j. The problem is to make explicit how $\mathcal{H}_R(j)$ and $\mathcal{H}_Y(j)$ are related to Munsell notation $(H_j\ V_j/C_j)$.[3,4] Perceived principal hue $\mathcal{H}_\alpha$ is a latent variable and has to be converted to an observable variable, $\xi_\alpha(j)$.

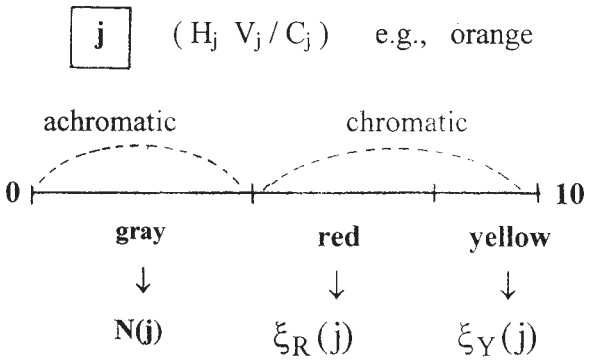

FIG. 1. Scaling procedure of principal hue components α in a Munsell chip j.

(H1): Converting $\mathcal{H}_\alpha$ in $P_j(H_j\ V_j/C_j)$ to data $\xi_\alpha(j)$ was made through the following assessment. Observers were asked to divide a given line as shown in Fig. 1, an example when j is an orange color. If chip j is not fully saturated orange, an observer makes two marks; one to show the degrees of achromaticness of that orange color, and the other to show the degrees of redness and of yellowness in the orange tint. The mean lengths of segments over observers are denoted as $N(j)$, and $\xi_\alpha(j)$. If j is of orange tint, $\xi_\alpha(j) > 0$ for α = R, Y and $\xi_\alpha(j) = 0$ for G and B. The total length of line is defined to be 10 and hence $0 \le \xi_\alpha(j) \le 10$ (Fig. 1).

(H2): The assessment was tried with five Munsell hue names (R, Y, G, B, P) and with four names (R, Y, G, B). It was found that the four is sufficient and these are defined as principal hues, α = R, Y, G, B. Since N and four ξ's are simultaneously assessed, the procedure is similar to what was called "5-category procedure" by Gordon and Abramov.[5–7] Usually, one or two $\xi_\alpha(j)$ are positive and remaining $\xi_\alpha(j)$ are 0.

(H3): In the (H, C) plane of the Munsell cylindrical coordinate system, the following four principal hue vectors $\mathbf{f}_\alpha$ were defined. Denote by $\hat{\xi}_\alpha(j)$ coordinates on $\mathbf{f}_\alpha$ of a point P_j in Munsell color solid $\{P_j\}_M$ regardless of value of V_j. If P_j is in the sector between $\mathbf{f}_\alpha$ and $\mathbf{f}_\beta$, then $\hat{\xi}_\alpha(j) > 0$, $\hat{\xi}_\beta(j) > 0$, and the other two $\hat{\xi}_\alpha(j) = 0$. If P_j is on $\mathbf{f}_\beta$, $\hat{\xi}_\alpha(j) = 0$. The direction of $\mathbf{f}_\alpha$ was so defined that data $\xi_\alpha(j)$ (>0) are most closely represented as a function of $\hat{\xi}_\alpha(j)$. Notice that, for example, $\hat{\xi}_R(j) > 0$ when P_j is between $\mathbf{f}_B$ and $\mathbf{f}_R$ as well as when P_j is between $\mathbf{f}_R$ and $\mathbf{f}_Y$. Then, the relationship between assessments $\xi_\alpha(j)$ (>0) and $\hat{\xi}_\alpha(j)$ ($\ge$0) is given by

$$\xi_\alpha(j) \approx \hat{\xi}\left[\hat{\xi}_\alpha(j)\right] = c_\alpha(V)\hat{\xi}_\alpha(j)^{\beta_\alpha(V)} \qquad (1)$$

Values of $c_\alpha(V)$, $\beta_\alpha(V)$ and RMS (root-mean-square of discrepancies between $\hat{\xi}_\alpha(j)$ and $\hat{\xi}[\hat{\xi}_\alpha(j)]$) are given in Table III in Indow.[4] For all values of α and V, exponent $\beta_\alpha(V) < 1.0$. Namely, when $\xi_\alpha(j)$ for $(H_j\ V/C_j)$ are plotted

against $\hat{\xi}_\alpha(j)$, points are along the convex upward curve $\hat{\xi}[\hat{\xi}_\alpha(j)]$ with the size of scatter indicated by RMS.

(H4): Because principal hue vectors have nothing to do with color mixing, it is not necessary to expect that a pair of complimentary colors to be represented by a bipolar vector passing through the achromatic point. Three vectors, $\mathbf{f}_R$, $\mathbf{f}_Y$, and $\mathbf{f}_G$, are approximately in the directions of 5R, 5Y, and 5G. On the other hand, $\mathbf{f}_B$ is not in the direction of 5B. It is almost in the direction of 2.5PB. In other words, 5B in the Munsell notation is not the most representative blue. This is not because P was not included in the assessment. Even if the assessment was made with five hue names, the situation was essentially the same. In this case, $\mathbf{f}_B$ was in the direction of 10PB, and $\mathbf{f}_P$ was just in the middle direction between $\mathbf{f}_R$ and $\mathbf{f}_B$.[4] This is one of the reasons that principal hues have been defined to be four.

(H5): Data d_{jk} in (D1), the scaled perceptual difference between $P_j(H_j\ V_j/C_j)$ and $P_k(H_k\ V_k/C_k)$ in the Munsell color solid, can be predicted[8,9] by a linear combination of $\Delta V = |V_j - V_k|$ and $\Delta\xi =$ sum of $|\xi_\alpha(j) - \xi_\alpha(k)|$.

Color Appearance Information in Spectral Reflectance *r* of Standard Chip

Romney and Indow[10–12] have recently analyzed the reflectance spectra $r_j(\lambda)$ of Munsell standard chips ($H_j\ V_j/C_j$). The research is based on two kinds of methodology. The first is approximation of $r_j(\lambda)$ by a limited basis-function expansion. Works of predecessors in this line of research are reviewed in Romney and Indow.[10,11] Since then, quite a few related articles have appeared in this journal and in others.[13–16] The second is multiple regressions of $r_j(\lambda)$ to underlying physiological processes.[17–19] Some new results in these two lines will be described below.

SINGULAR VALUE DECOMPOSITION

A rectangular matrix $\mathbf{X}_{N\times M}$, $N > M$, of rank m ($\leq M$) can be written in a form $\mathbf{U}\Delta\mathbf{V}^T$ where $\mathbf{U}_{N\times m}$ and $\mathbf{V}_{M\times m}$ are orthonormal matrices and $\Delta_{m\times m}$ is a diagonal matrix. The reflectance spectrum $r_j(\lambda)$ of a Munsell chip j is a series of M values with an appropriate step of wavelength λ. If we take N standard chips, we have a rectangular matrix $\mathbf{S}_{N\times M}$ and it can be approximated by $\mathbf{PW}^T$ where $\mathbf{P}_{N\times m} = \mathbf{U}\Delta$ and $\mathbf{W}_{M\times m} = \mathbf{V}$. The matrix $\mathbf{P}$ defines a configuration of N points in an m-dimensional space and $\mathbf{W}$ gives a series of M points representing wavelength λ in the same space. These $\mathbf{P}$ and $\mathbf{W}$ can be transformed by an orthogonal rotation in that space to $\overline{\mathbf{P}}$ and $\overline{\mathbf{W}}$ so that this N point configuration $\overline{\mathbf{P}}$ most resembles the structure $\{P_j\}_M$ of Munsell color solid. After the transformation, the approximation still holds, $\mathbf{S} \approx \mathbf{PW}^T = \overline{\mathbf{P}}\ \overline{\mathbf{W}}^T$.

With $[r_j(\lambda)]$ of the Munsell color book (1976 matte edition), the decomposition was tried in two ways.

1. Reflectance spectra of all standard chips,[10] $s_{j\mu} = r_{j\mu}$, $j = 1, \ldots, 1269$.

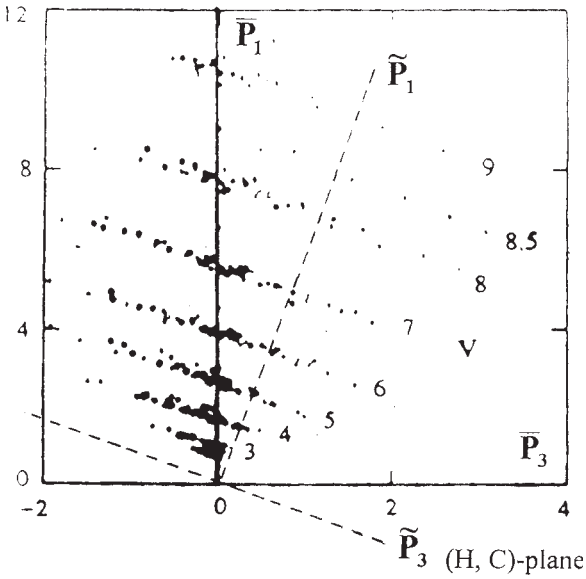

FIG. 2. Configuration in the $(\overline{P}_1, \overline{P}_3)$ plane of $\overline{P}_{370\times3}$ obtained by singular value decomposition (II). Points representing chips (H_j V/C_j) of the same V form thin layers. $\overline{\mathbf{P}}$ is rotated to $\tilde{\mathbf{P}}$ so that its first column vector $\tilde{P}_1$ and $(\tilde{P}_2, \tilde{P}_3)$ plane respectively represent Munsell V and Munsell (H, C) plane.

2. Spectra of reflected light from 5H standard chips,[11] $s_{j\mu} = r_{j\mu} \times e_\mu$ $j = 1, \ldots, 370$, (5R V/C), (5YR V/C), $\ldots\ldots$, (5RP V/C), $V = 2.\ 2.5, 3, 4, 5, 6, 7, 8, 8.5, 9$.

C covers the whole range of chroma, and 10 achromatic chips.

e_μ is the spectral radiant power distribution of the standard illuminant D65.

In both cases, the spectrum was limited between 430 to 660 nm with 1 nm intervals and hence $M = 231$. It was found that $m = 3$ is sufficient for an approximation.

$$\mathbf{S} = (s_{j\mu}) \approx \hat{\mathbf{S}} = (\hat{s}_{j\mu}) = \overline{\mathbf{P}}\ \overline{\mathbf{W}}^T,\ \overline{\mathbf{P}} = (\overline{p}_{j\gamma}),\ \overline{\mathbf{W}} = (\overline{w}_{\mu\gamma})$$
$$\mu = 1, 2, \ldots\ldots\ldots, 231,\ \gamma = 1, 2, 3. \quad (2)$$

Figure 5 of Ref. 10 on decomposition I shows with 40 examples, how well $s_{j\mu}$ is reproduced by $\hat{s}_{j\mu}$. The first axis $\overline{P}_1$ of $\overline{\mathbf{P}}$ was defined so as to represent lightness direction. Figure 2 shows a plot of $\overline{p}_{j1}$ against $\overline{p}_{j3}$ of decomposition II.[11] Points $\overline{P}_j$ representing (H_j V/C_j) of the same level of V form a thin layer, implying that all are in the same plane $(\overline{P}_2, \overline{P}_3)$. These layers are not orthogonal to $\overline{P}_1$ axis but all are almost parallel. This situation is the same in decomposition I.[10] It was pointed out in the preceding articles that the tilt of chips of the same V with regard to $\overline{P}_1$ of planes $(\overline{P}_2, \overline{P}_3)$ is due to the following circumstances. In Munsell V, the CIE luminosity function $\overline{y}_\mu$ is taken into account, whereas $\overline{p}_{j1}$ represents the mean of $s_{j\mu}$ over μ. In the same 3D space in which $(\overline{p}_{j1}, \overline{p}_{j2}, \overline{p}_{j3})$ are plotted, we can include $(\overline{w}_{\mu1}, \overline{w}_{\mu2}, \overline{w}_{\mu3})$ with an appropriate adjustment of size. The latter appears as a curve almost orthogonal to $\overline{P}_1$.

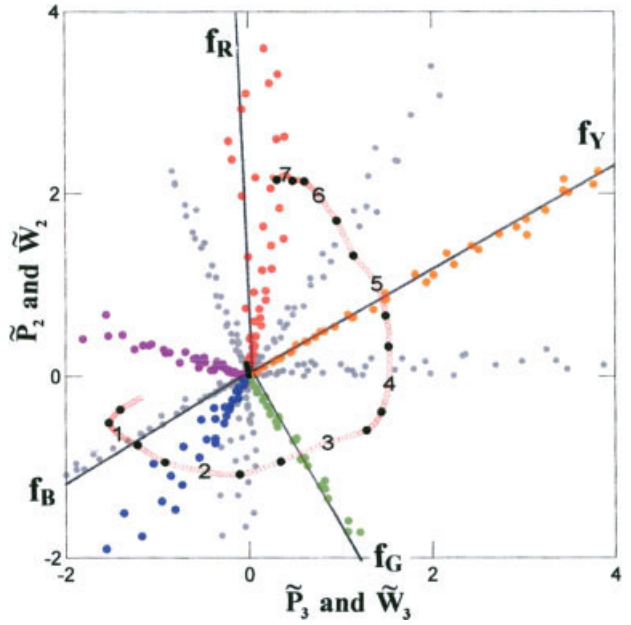

FIG. 3. Configuration $\tilde{\mathbf{P}}$ of 370 (H_j V_j/C_j) and spectral curve $\tilde{\mathbf{W}}$ for 430 to 660 nm in $(\tilde{P}_2, \tilde{P}_3)$ plane. Points of the same H, (H V_j/C_j) are around radial lines $\tilde{P}(H)$ from the origin (achromatic color). Points of 5 Munsell hues are indicated by corresponding colors except 5Y. 5Y is represented by orange. Points of five intermediate hues, such as 5YR, are all gray. As to numbers on the spectral curve $\tilde{\mathbf{W}}$, see the text. Vectors $\mathbf{f}_\alpha$ representing principal hues α defined by assessment experiments are superimposed on $\tilde{\mathbf{P}}$.

As indicated by the dashed lines in Fig. 2, we can introduce a new orthogonal coordinate axes $(\tilde{P}_1, \tilde{P}_2, \tilde{P}_3)$ in which $\tilde{P}_1$ is almost orthogonal to all layers of points of the same V. The new axis $\tilde{P}_1$ is tilted to $\overline{P}_1$ by 38° (the angle in Fig. 2 is not 38° because scales of x-axis and y-axis not identical). Intersections of each layer of points (H_j V/C_j) with $\tilde{P}_1$ are exactly given by

$$V = 5.21\ \tilde{P}_1^{0.33} - 1.90 \tag{3}$$

This is the same form with the relationship between Munsell V and the CIE luminance factor Y, with the same value of exponent, 0.33. Since the new plane $(\tilde{P}_2, \tilde{P}_3)$, orthogonal to $\tilde{P}_1$, should represent (H, C), all points $(\overline{p}_{j1}, \overline{p}_{j2}, \overline{p}_{j3})$ and $(\overline{w}_{\mu 1}, \overline{w}_{\mu 2}, \overline{w}_{\mu 3})$ were projected on this plane along $\tilde{P}_1$. Figure 3 shows $(\tilde{p}_{j2}, \tilde{p}_{j3})$ and $(\tilde{w}_{\mu 2}, \tilde{w}_{\mu 3})$ thus obtained. Points of 5 Munsell hues are indicated by corresponding colors, except 5Y (this is represented by orange). Points of five intermediate hues, for example, 5YR, etc. are all gray. Points $\tilde{P}_j$ (H V_j/C_j) of the same H approximately form a radial line $\tilde{P}(H)$ from the origin in which all 10 achromatic samples are represented. The spectral positions $(\tilde{w}_{\mu 2}, \tilde{w}_{\mu 3})$, from 430 to 660 nm, are shown by a curve around the origin and the numbers on it indicate intervals of 30 nm beginning in the lower left, where 1 indicates 460 nm.

The four principal hue vectors $\mathbf{f}_\alpha$ [(H3) in the preceding section] were first superimposed on the plane $(\overline{P}_2, \overline{P}_3)$ and then projected to the new plane $(\tilde{P}_2, \tilde{P}_3)$ along $\tilde{P}_1$ (Fig. 3). The relationship between projected $\mathbf{f}_\alpha$, α = R, Y, G, B, and Munsell H is almost the same as the relationship between unique hues and Munsell H in Figs. 4–11 of Kuehni.[20] From now on, projected $\mathbf{f}_\alpha$ are used as the oblique coordinate system in the $(\tilde{P}_2, \tilde{P}_3)$ plane, and Fig. 4 shows how to define coordinates ξ on $\mathbf{f}$. For points in a sector delimited by $\mathbf{f}_\alpha$ and $\mathbf{f}_\beta$, ξ_α, $\xi_\beta > 0$. For these points, ξ on the remaining $\mathbf{f}$'s are undefined. If point is on $\mathbf{f}_\beta$, $\xi_\alpha = 0$. Coordinate of a point λ on the spectral curve $(\tilde{w}_{\mu 2}, \tilde{w}_{\mu 3})$ is denoted as $\xi_\alpha(\lambda) \geq 0$. Figure 5 shows $\xi_\alpha(\lambda)$ with the corresponding color, except Y. Y is represented by orange. The curves depict roles of two sets of opponent processes, R versus G and Y versus B, in the spectrum of reflected light. In the present article, however, it is more appropriate to depict these roles as functions of Munsell hue notation, H. Coordinate of intersection of a hue line $\tilde{P}(H)$ with the spectral curve is denoted as $\xi_{0\alpha}(H) \geq 0$ (Fig. 4). Figure 6 shows these curves. Values of $\xi_{0\alpha}$(5R) to $\xi_{0\alpha}$(7.5PB) could be read directly from Fig. 3. Referring to Fig. 3, we estimated the parts of $\xi_{0R}(H)$, $\xi_{0Y}(H)$, and $\xi_{0B}(H)$ in the extra-spectral region from 5P to 2.5R by interpolation in Fig. 6. Placing 5R on the both ends of abscissa makes the interpolation easier.

Singular value decomposition of $\mathbf{S} = (s_{j\mu}) \approx \tilde{\mathbf{P}}\tilde{\mathbf{W}}^{\mathrm{T}}$ provides us with two sets of separate information in the space spanned by three axes, γ = 1, 2, 3. One is $\tilde{\mathbf{P}} = (\tilde{p}_{j\gamma})$ showing the structure of Munsell chip configuration in a 3D space and the other is $\tilde{\mathbf{W}} = (\tilde{w}_{\mu\gamma})$, representing such characteristic of λ that, when modulated by $\tilde{p}_{j\gamma}$, determines the appearance of (H_j V_j/C_j). Curves $\xi_{0\alpha}(H)$ in Fig. 6 were obtained by combining $\tilde{\mathbf{W}}$ with $\mathbf{f}_\alpha$ described in (H3) in Introduction. Implications of $\xi_{0\alpha}(H)$ will be discussed in the next section.

PRINCIPAL HUE COMPONENTS

In Eq. (1) of (H3), scaled principal hue component α in Munsell standard chip j, $\xi_\alpha(j)$, is approximated by a power function of $\tilde{\xi}_\alpha(j)$, coordinate of P_j for (H_j V_j/C_j) on $\mathbf{f}_\alpha$ in

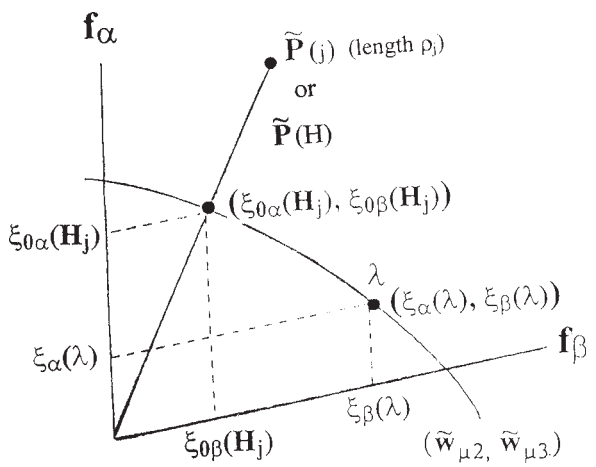

FIG. 4. Coordinates ξ of points on oblique coordinate axes $\mathbf{f}$ in $(\tilde{P}_2, \tilde{P}_3)$ plane.

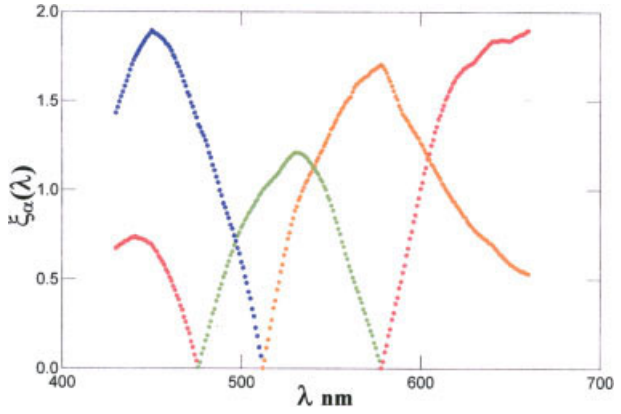

FIG. 5. Principal hue curves $\xi_\alpha(\lambda)$, coordinates on $\mathbf{f}_\alpha$ of λ on spectral curve (see Fig. 4). Yellow is represented by orange.

(H3). Hence, it is expected that the same approximation will hold if coordinate of $\tilde{\mathrm{P}}(j)$ on $\mathbf{f}_\alpha$ in the plane $(\tilde{\mathrm{P}}_2, \tilde{\mathrm{P}}_3)$ is used as a predicting variable for data $\xi_\alpha(j)$. From Fig. 4, the following predictor $\tilde{\xi}_\alpha(j)$ was defined.[12] Denote by ρ_j the length of radial line to $\tilde{\mathrm{P}}(j)$. Then a question arises whether the following approximation is better than Eq. (1).

$$\xi_\alpha(j) \approx \hat{\xi}\left[\tilde{\xi}_\alpha(j)\right] = c_\alpha(V)\tilde{\xi}_\alpha(j)^{\beta_\alpha(V)}$$
$$\tilde{\xi}_\alpha(j) = \xi_{0\alpha}(H_j) \times \rho_j \qquad (4)$$

Figure 7 shows plots of $\xi_\alpha(j)$ (>0) and curve $\hat{\xi}[\tilde{\xi}_\alpha(j)]$ against $\tilde{\xi}_\alpha(j)$ (≥ 0) in which numbers indicate V_j. Values of $\beta_\alpha(V)$ and of root-mean-square RMS are given in Table I.

$$\mathrm{RMS} = \sqrt{\frac{1}{N}\left(\xi_\alpha(j) - \hat{\xi}\left[\tilde{\xi}_\alpha(j)\right]\right)^2},$$

N is the number of points in each level of V

Parameter $c_\alpha(V)$ in Eq. (4) is only for adjusting the difference of scales between $\xi_\alpha(j)$ and $\tilde{\xi}_\alpha(j)$. Exponent $\beta_\alpha(V)$ determines the shape of curve $\hat{\xi}[\tilde{\xi}_\alpha(j)]$ and is independent of the scales. For comparison, values of $\beta_\alpha(V)$ and RMS for $\hat{\xi}[\tilde{\xi}_\alpha(j)]$ in Eq. (1) in (H3) are included in Table I. All curves $\hat{\xi}(\tilde{\xi}_\alpha(j))$, except Y of two high levels of V, are convex upward ($\beta_\alpha(V) < 1.0$). In the case of G, RMS's for Eq. (4) are systematically larger than those of (1). In remaining cases, it is difficult to say which approximation, (1) or (4), is better. The behavior of $\hat{\xi}(\tilde{\xi}_\mathrm{Y}(j))$ is very different from others. It is almost straight and convex downward for $7V$ and $8V$. This tendency is not observed with $\hat{\xi}[\tilde{\xi}_\mathrm{Y}(j)]$ in Eq. (1).

That we have to use power functions, rather than linear functions, to predict data $\xi_\alpha(j)$ is not because a single set of $\mathbf{f}_\alpha$ is used for all $(H_j\ V_j/C_j)$ or not because four, instead of five, principal hues are used. Even if separate sets of $\mathbf{f}_{\alpha v}$ are defined for each level of V or even if $\mathbf{f}_\mathrm{P}$ for Munsell P is included, the situation is the same.[4]

CONTRIBUTION OF THREE CONES

The first step of visual processes, when observing a Munsell chips, is excitations of cones in the retina. Cones in human retina are of three types. They are referred to as long-, middle- and short-wavelength-sensitive (L, M, and S), according to the spectral positions of their peak sensitivities. Let us denote by $c_{q\mu}$, $q = \mathrm{L}, \mathrm{M}, \mathrm{S}$, their sensitivity curves (2°), with 1–nm intervals, obtained by Stockman and Sharpe.[21] Each is normalized by putting $c_{q\mu} = 1.0$ at its peak. In each $(H_j\ V_j/C_j)$, spectrum $s_{j\mu}$ in Eq. (2) were regressed on $c_{q\mu}$.

$$s_{j\mu} \approx \hat{\mathrm{s}}_{j\mu} = a_j + \sum\nolimits_\mathrm{q} b_{j\mathrm{q}} \mathrm{c}_{\mathrm{q}\mu}^{0.33} \qquad (5)$$

The use of cube root transformation is an analogy from Eq. (3). Adams[22] used the same analogy when he defined his "chromatic values" for CIE X and CIE Z with the same functional form between Munsell V and CIE Y. Other reasons are given in Indow and Romney.[12] The parameter a_j is the mean level of $s_{j\mu}$ over μ. It depends upon $(H_j,\ C_j)$ how V_j is related to a_j. The coefficients $b_{j\mathrm{q}}$ shows how cube root of $c_{q\mu}$ are involved in determining the form of spectrum around a_j. The curve $(s_{j\mu}\ \ a_j)$ is related to $(H_j,\ C_j)$. We tried to define the relative contributions among three cones by

$$B_{j\mathrm{q}} = \frac{b_{jq}}{\sum_q |b_{jq}|}, \qquad q = \mathrm{L}, \mathrm{M}, \mathrm{S} \qquad (6)$$

Regression (5) was tried with spectra of reflected light of all standard chips under D65; $s_{j\mu} = r_{j\mu} \times e_\mu$, $j = 1, \ldots, 1269$, $\mu = 1, \ldots, 231$. As examples, B_{jq} for chips of $7V$ are shown in Fig. 8. Numbers in the plots are values of C_j ($10C$ and $12C$ are denoted by 0 and circle). In each q, points B_{jq} for $(H_j\ 7V/C_j)$ form a single curve for all values of C_j (>2). The situation is the same for $(H_j\ V_j/C_j)$ for other values of V. In other word, B_{jq} are almost independent of V_j and C_j in the main part of Munsell color solid. Figure 9 shows how a_j in Eq. (5) varies according to V_j and C_j. The regression was also tried without the constant term a_j in Eq. (5). In this case, B_{jq} are much more V_j and C_j dependent.

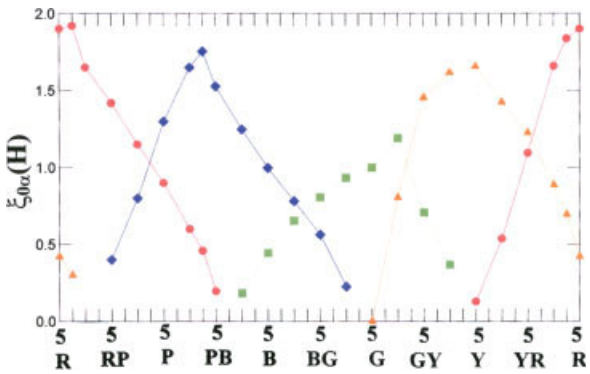

FIG. 6. Principal hue curves $\xi_{0\alpha}(H)$, coordinate on $\mathbf{f}_\alpha$ of intersection of $\tilde{\mathrm{P}}(H)$ and spectral curve $\tilde{\mathbf{W}}$ (see Fig. 4). Yellow is represented by orange.

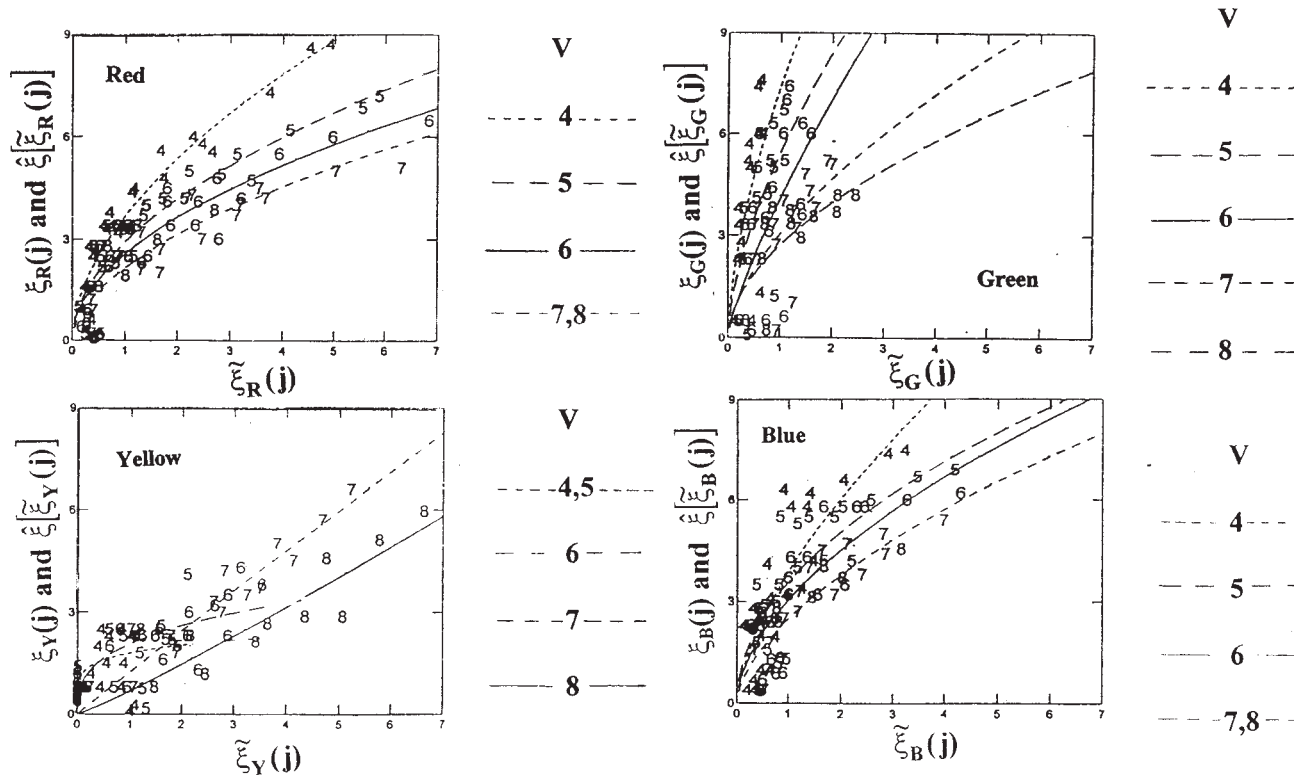

FIG. 7. Scaled principal hue components $\xi_\alpha(j)$ obtained by assessment experiments for Munsell chip (H_j V_j/C_j) plotted against $\tilde{\xi}_\alpha(j)$. $\tilde{\xi}_\alpha(j)$ and $\hat{\xi}[\tilde{\xi}_\alpha(j)]$ are defined in Eq. (4). Numbers in the plots indicate V_j.

Let us denote by $B_q(H)$ mean values of B_{jq} over V_j and C_j. Equation (6) implies that, in each j, $\sum_q |B_{jq}| = 1$. However, $\sum_q |B_q(H)| < 1$ unless all B_{jq} to be averaged in each q are of the same sign. In fact, the sum was equal to or close to unity. Under various conditions, $B_q(H)$ were determined and plotted against H. Various conditions mean the following variations; regression with or without a_j in (5), two definitions of $s_{j\mu}$,(= $r_{j\mu}$ as Decomposition I in Eq. (2) or $r_{j\mu} \times e_\mu$ as Decomposition II) and various ranges of V_j and C_j over which means are taken. Figure 10 shows $B_q(H)$ as means of B_{jq} with a_j for the above mentioned set of $s_{j\mu} = r_{j\mu} \times e_\mu$ and the range ($C > 2$ and all levels of V). Figure 11 shows $B_q(H)$ with a_j for reflectance spectra, $s_{j\mu} = r_{j\mu}$, and the range ($C \leq 8$, all levels of V) (Fig. 4 in Romney *et al.*[18]). The reason for showing Fig. 11 herein is that these curves $B_q(H)$ are most consistent with curves $\xi_{0\alpha}(H)$ in Fig. 6 and with predictions from a model of higher order color mechanism to be stated below.

Figure 12 is a schematic representation of an opponent-color model. Derrington *et al.*,[23] used this model to describe chromatic mechanisms in lateral geniculate nucleus of macaque and Krauskopf[24–26] used this model to account for human psychophysical experiments. Figure 12(A) is taken from Boynton and Kambe.[27] A luminance channel sends pooled outputs from L and M cones. S cones make no contribution to luminance. Signals sent through two opponent-color channels determine the chromatic appearance of color. Balance between outputs from L cones and from M cones designates whether the color is reddish (r) or greenish (g) whereas balance between the pooled outputs from L, M cones and outputs from S cones designates whether the color is bluish (b) or yellowish (y). We are concerned with curves $B_q(H)$ and $\xi_{0\alpha}(H)$. Both are independent of lightness. Hence, let us consider an iso-luminance plane of the model in which L + M is constant. Independence of the two opponent channels is schematized by two

TABLE I. Values of exponents, $\beta(V)$, and indices of fit, RMS, of Eq. (4) and Eq. (1) to assessment data, $\xi_\alpha(j)$, α = R, Y, G, B.

		Eq. (4)		Eq. (1)	
	V	β(V)	RMS	β(V)	RMS
R	4	0.54	0.78	0.88	0.88
	5	0.52	0.68	0.69	0.85
	6	0.50	0.51	0.66	0.60
	7, 8	0.54	0.69	0.61	0.49
Y	4, 5	0.17	0.77	0.51, 0.73	0.28, 0.45
	6	0.33	0.66	0.79	0.48
	7	0.97	0.52	0.77	0.67
	8	1.10	0.69		
G	4	0.64	1.81	0.84	0.89
	5	0.68	1.46	0.62	0.86
	6	0.79	1.69	0.62	0.90
	7	0.63	1.10	0.67	0.65
	8	0.55	0.81		
B	4	0.64	1.13	0.67	1.45
	5	0.50	1.00	0.64	1.04
	6	0.57	0.96	0.78	0.54
	7, 8	0.60	0.69	0.70	0.45

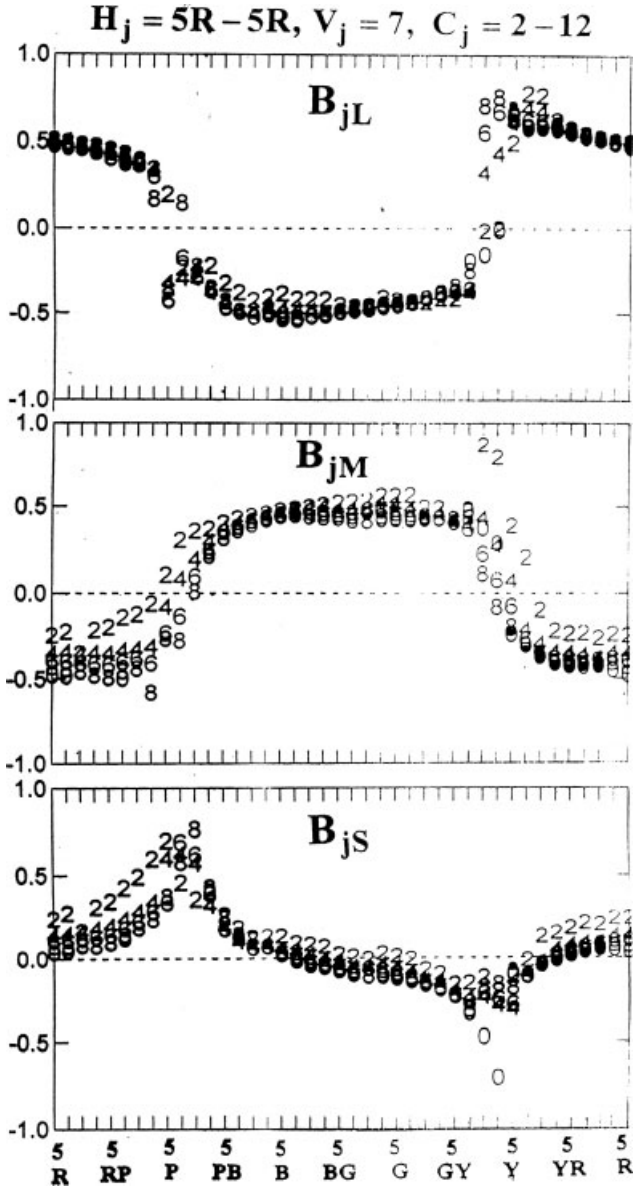

FIG. 8. Plots of B_{jq} against H_j, Eq. (6). B_{jq} is relative involvements of activity of cone q (L, M, S) in the processes caused by spectra of reflected light $s_{j\mu} = r_{j\mu} \times e_\mu$, $j = 1, \ldots, 1269$, $\mu = 1, \ldots, 231$. Numbers in the plots are values of C_j (10*C* and 12*C* are denoted by 0 and circle).

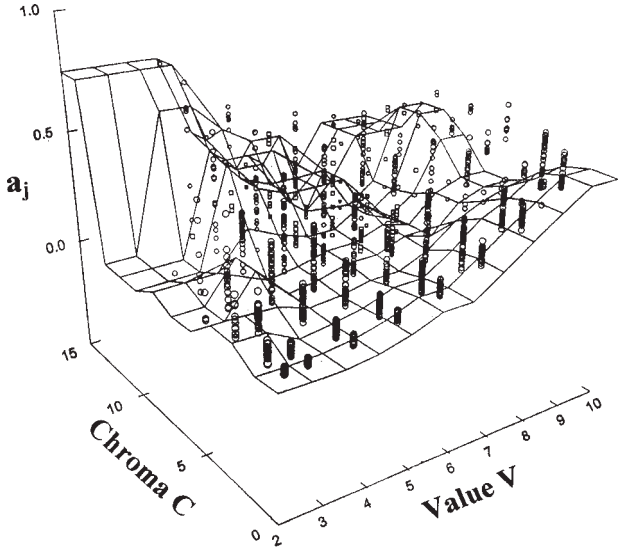

FIG. 9. Values of constant term a_j in regressions of $s_{j\mu} = r_{j\mu} \times e_\mu$ on activities of cone q, Eq. (5).

orthogonal axes in Fig. 12(B). Munsell hue names are superimposed under the assumption that the axis (r−g) corresponds to 5R and 5BG.

Comparison of predictions from this model and curves $B_q(H)$ is made from the following view point. Each $B_q(H)$ is based on the normalized cone sensitivity curves $c_{q\mu}$ with its own unit [Eq. (5)]. Hence, $B_q(H)$ shows, in each cone q, how strength of the output changes according to H. However, we cannot compare three values of $B_q(H)$ at the same position H because the respective units are different. Suppose that $c_{L\mu}$, $c_{M\mu}$, $c_{S\mu}$ are given with the same common unit of strength. The change of unit will affect amplitude of each curve $B_q(H)$ around the 0-level (the horizontal dashed line in Figs. 10 and 11). But, positions on the abscissa of its positive and negative peaks and its zero-crossings may be immune from the change.

DISCUSSION CONCERNING B_q(H) AND $\xi_{0\alpha}$ (H)

1. The model predicts that at 5R [$B_S(H) = 0$, $B_L(H) > 0$, and $B_M(H) < 0$] and in the vicinity of 5BG [$B_S(H) = 0$, $B_L(H) < 0$, and $B_M(H) > 0$]. This is what happens in Figs. 10 and 11. In Fig. 6, $\xi_{0R}(H)$ is maximum around 5R and $\xi_{0G}(H) = \xi_{0B}(H)$ around 5BG.
2. As predicted from the model, $B_S(H)$ in Fig. 11 are negative while H is YR, Y, GY, G. In between 5Y and 5GY, $B_S(H)$ is minimum and $B_L(H)$, $B_M(H)$ cross the 0-line. This is the region at which $\xi_{0Y}(H)$ is maximum in Fig. 6. $B_q(H)$ in Fig. 10 does not exactly follow this pattern.
3. As predicted from the model, $B_S(H)$ in Fig. 11 are positive while H is B, PB, P. Its peak is at about 7.5PB. This is position at which B_M(H) crosses the 0-line and

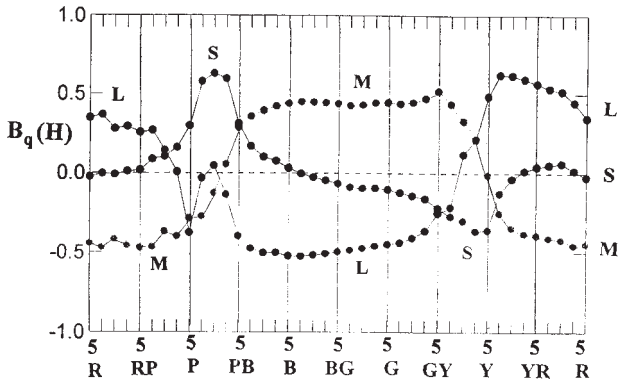

FIG. 10. $B_q(H)$, means over V_j and C_j of B_{jq} [Eq. (5) $s_{j\mu} = r_{j\mu} \times e_\mu$ with a_j) in the range that $C > 2$ and V of all levels.

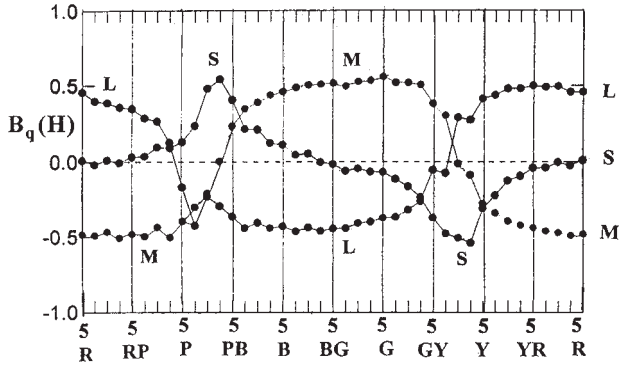

FIG. 11. $B_q(H)$, means over V_j and C_j of B_{jq} [Eq. (5) $s_{j\mu} = r_{j\mu}$ with a_j] in the range that $C \leq 8$ and V of all levels.

$\xi_{0B}(H)$ is at peak in Fig. 6. In Fig. 10, $B_S(H)$ are also positive while H is B, PB, P. Its peak is at about 10PB and in its vicinity, $B_L(H)$, $B_M(H)$ cross the 0-line. However, $B_L(H)$ becomes negative again around 5P.

4. The peak of $\xi_{0G}(H)$ is around 10GY in Fig. 6. Around this region, both in Figs. 10 and 11, [$B_L(H) < 0$, $B_M(H) > 0$, and $B_S(H) < 0$]. In Fig. 11, $B_L(H)$ and $B_S(H)$ happen to have the same absolute value in this region. For the reason stated above, however, it is questionable whether this is meaningful or not.

The model of opponent colors we considered herein is for aperture colors. In the processes determining appearance of surface colors, more steps than depicted in Fig. 12 will be involved. In order to shed light on this problem, we have to continue to compare its predictions with results based on surface colors such as Figs. 6, 10, and 11.

Among all $B_q(H)$'s we tried under various conditions, the curves $B_q(H)$ in Fig. 11 are most consistent with predictions from the model and with curves $\xi_{0\alpha}(H)$ in Fig. 6. Though B_{jq} for $C_j > 8$ are excluded in defining $B_q(H)$, these are small in number and do not affect the general form of $B_q(H)$. The curves $B_q(H)$ in Fig. 11 are for reflectance spectra of chips, $s_{j\mu} = r_{j\mu}$, which are independent of illumination. That most consistent results happened to be obtained with $r_{j\mu}$ could be fortuitous, but we need to pay attention to the following possibility. As appearance of other surface colors, Munsell standard chips appear the same under the wide range of change in illumination spectrum. Hence, the characteristic of stimulus that determines the appearance of chips is captured, not in the spectra of the reflected light under a specific illumination, but in the reflectance spectra of chips themselves.

SUMMARY OF STUDIES ON MUNSELL SOLID

Studies based on scaling perceptual differences δ_{jk} between Munsell standard chips j and k have made it clear that chips are embeddable as a configuration of points $\{P_j\}$ in a 3D space with locally Euclidean metric. However, in order to accumulate through this approach sufficient information that is necessary to provide Munsell color solid with a unified distance scale, tremendous amount of experimentation will be necessary. It is more practical to examine the status quo of Munsell standard color chips. This approach was tried in two ways. One is to scale as $\xi_\alpha(j)$ principal hue components $H_\alpha(j)$ that we perceive in standard chips j in the main part of Munsell color solid. In this way, four principal hue vectors $\mathbf{f}_\alpha$ were identified. The other approach is to analyze such information in reflectance spectra $r_j(\lambda)$ in all standard chips j that is related to its appearance. Through application of singular value decomposition to a matrix $(s_{j\mu})$, $s_{j\mu} = r_{j\mu}$ or $r_{j\mu} \times e_\mu$, where $r_{j\mu}$ is spectral reflectance of chips j and e_μ is the spectral radiant power distribution of D65, we obtained in a 3D-space a configuration of points $\tilde{\mathbf{P}}$ representing the structure of Munsell color solid and a plane $(\tilde{\mathbf{w}}_{\mu 2}, \tilde{\mathbf{w}}_{\mu 3})$ representing such characteristic of wavelength μ that determines the appearance of chips $(H_j\ V_j/C_j)$.

Combining $\mathbf{f}_\alpha$ and $(\tilde{\mathbf{w}}_{\mu 2}, \tilde{\mathbf{w}}_{\mu 3})$, we defined four curves $\xi_{0\alpha}(H)$ that represent appearance of redness, yellowness, greenness, and blueness in the spectrum of reflected light

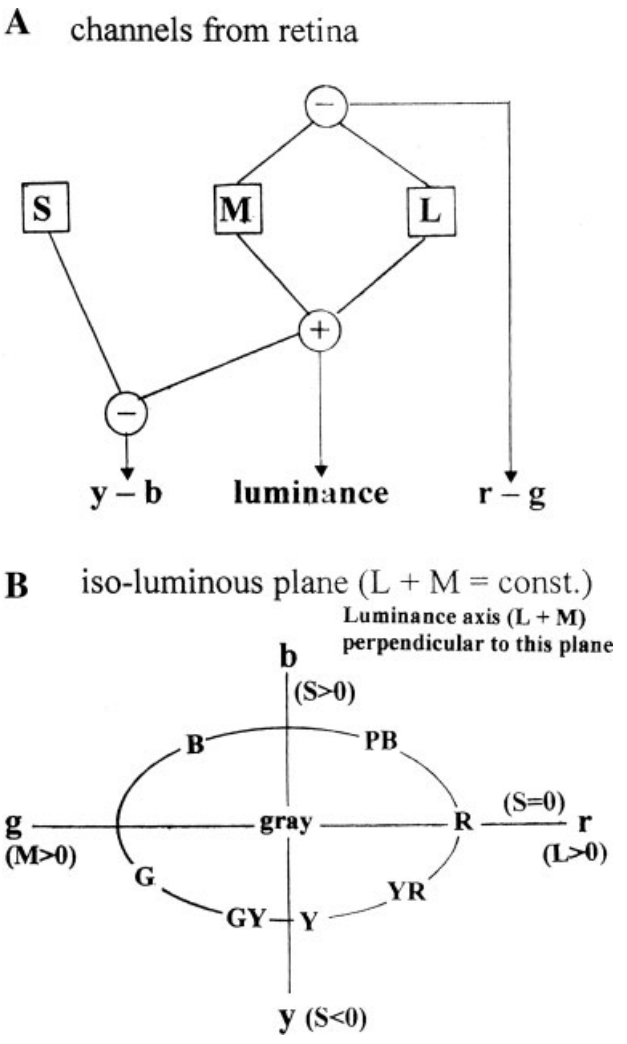

FIG. 12. A model of higher order color mechanism.

from (H V_j/C_j) under D65 (Fig. 6). Denote $\tilde{\xi}_\alpha(j)$ $\xi_{0\alpha}(H) \times \rho_j$ [Eq. (4)] where ρ_j is explained in Fig. 4. Then, assessment data of principal hue components $\xi_\alpha(j)$ were shown to be power functions of $\tilde{\xi}_\alpha(j)$ (Fig. 7 and Table I). Data $\xi_\alpha(j)$ are also power functions of coordinates $\hat{\xi}_\alpha(j)$ of (H_j V_j/C_j) on $\mathbf{f}_\alpha$ [Eq. (1) in (H1)]. In both cases, exponent $\beta_\alpha(V)$ of power function changes its values according to principal hue α and Munsell value V. As emphasized by Nayatani in discussion on his NT-system,[28,29] nonlinearity of this type seems to be necessary to relate (H_j V_j/C_j) to its perceptual appearance.

From regression analysis of each $s_{j\mu}$ on cone sensitivity curves $c_{q\mu}$, q = L, M, S, we defined relative involvements q cone, $B_q(H)$, [Eq. (6)]. $B_q(H)$ are basic characteristic in Munsell Hue from which appearance of (H_j V_j/C_j) is predicted. Two examples are shown in Figs. 10 and 11.

The curves $\xi_{0\alpha}(H)$ in Fig. 6 can be a norm for deciding what is the best way to represent relative involvements of the three cones and also which model is most plausible for the processes that are directly related to appearance of Munsell standard chips. As an example of such models, one used by Derrington *et al*. was taken up (Fig. 12) and predictions from this model were compared with $\xi_{0\alpha}(H)$ in Fig. 6 and $B_q(H)$ in Figs. 10 and 11. The main purpose of this article is to show the possibility of these comparisons. It is worthwhile mentioning that we came across such a finding. If we accept the model of Fig. 12, Munsell standard chips have been selected so that the characteristic determining appearance of chips in terms of this model lies in the reflectance spectra themselves rather than in spectra of the light reflected from them under a specific illumination.

1. Indow T. Multidimensional studies of Munsell color solid. Psychol Rev 1988;95:456–470.
2. Indow T. Predictions based on Munsell notation. I. Perceptual color differences. Color Res Appl 1999;24:10–18.
3. Indow T. Psychologically unique hues in aperture and surface colors. Farbe 1987;34:253–260.
4. Indow T. Predictions based on Munsell notation. II. Principal hue components. Color Res Appl 1999;24:19–32.
5. Gordon J, Abramov I. Scaling procedures for specifying color appearance. Color Res Appl 1988;13:146–152.
6. Gordon J, Abramov I, Chan H. Describing color appearance: Hue and saturation scaling. Percept Pschophys 1994;54:27–41.
7. Abramov I, Gordon J. Scaling unique hues. J Opt Soc Am A 2005;22:2143–2153.
8. Indow T. Principal hue curves and color difference. Color Res Appl 1999;24:266–279.
9. Indow T. Color difference predicted by color component differences. Color Res Appl 2002;27:425–429.
10. Romney AK, Indow T. Munsell reflectance spectra represented in three-dimensional Euclidean space. Color Res Appl 2003;28:182–196.
11. Romney AK, Indow T. A model for the simultaneous analysis of reflectance spectra and basis factors of Munsell color samples under D65 illlumination in three-dimensional Euclidean space. Proc Natl Acad Sci USA 2002;99:11543–11546.
12. Indow T, Romney AK. Singular value decomposition of Munsell color samples: Principal hue components. AIC Color 05, The 10th Congress of the International Color Association, Granada, 2005. pp 25–28.
13. Fairman HS, Brill MH. The principal components of reflectance. Color Res Appl 2004;29:104–110.
14. Worthey JA, Brill MH. Principal components applied to modeling: Dealing with mean vector. Color Res Appl 2004;29:261–266.
15. Brill MH. A non-PC look at principal components. Color Res Appl 2003;28:69–71.
16. Oxtoby EK, Foster DH. Perceptual limits on low-dimensional model of Munsell reflectance spectra. Perception 2005;34:961–966.
17. Romney AK, Indow T. Estimating physical reflectance spectra from human colo-matching experiments. Proc Natl Acad Sci USA 2002; 99:14607–14610.
18. Romney AK, D'Andrade RG, Indow T. The distribution of response spectra in the lateral geniculate nucleus compared with reflectance spectra of Munsell color chips. Proc Natl Acad Sci USA 2005;102: 9720–9725.
19. Romney AK, D'Andrade RG. Modeling lateral geniculate nucleus cell response spectra and Munsell reflectance spectra with cone sensitivity curves. Proc Natl Acad Sci USA 2005;102:16512–16517.
20. Kuehni RG. Color Space and its Divisions: Color Order from Antiquity to the Present. Hoboken, New Jersey: Wiley; 2003.
21. Stockman A, Sharpe LT. (2000) 2-deg (from 10-deg) cone fundamentals.http://cvision.ucsd.edu/database/text/cones/linss2_10e 1.txt
22. Adams EQ. X-Z planes in the 1931 I.C.I. systems of colorimetry. J Opt Soc Am 1942;32:168–173.
23. Derrington AH, Krauskopf J, Lennie P. Chromatic mechanisms in lateral geniculate nucleus of macaque. J Physiol 1984;357:241–265.
24. Krauskopf J, Williams DR, Heeley DW. Cardinal directions of color space. Vision Res 1982;22:1123–1131.
25. Krauskopf J, Wu HJ, Farell B. Coherence, cardinal directions, and higher-order mechanisms. Vision Res 1996;36:1235–1245.
26. Krauskopf J. Higher order color mechanism. In: Gegenfurtner KR, Sharpe LT, editors. Color Vision. Cambridge: Cambridge University Press; 1999. p 303–316.
27. Boynton RM, Kambe N. Chromatic difference steps of moderate size measured along theoretically critical axes. Color Res Appl 1980;5: 13–23.
28. Nayatani Y. Proposal of an opponent-colors system based on color appearance and color vision studies. Color Res Appl 2004;29:135–150.
29. Nayatani Y. Why two kinds of color order systems are necessary? Color Res Appl 2005;30:295–303.